

Article

# Hypergolics in Carbon Nanomaterials Synthesis: New Paradigms and Perspectives

Nikolaos Chalmes <sup>1</sup>, Konstantinos Spyrou <sup>1</sup>, Konstantinos C. Vasilopoulos <sup>1</sup>, Athanasios B. Bourlinos <sup>2,\*</sup>, Dimitrios Moschovas <sup>1</sup>, Apostolos Avgeropoulos <sup>1</sup>, Christina Gioti <sup>1</sup>, Michael A. Karakassides <sup>1</sup> and Dimitrios Gournis <sup>1,\*</sup>

<sup>1</sup> Department of Materials Science and Engineering, University of Ioannina, 45110 Ioannina, Greece; chalmesnikos@gmail.com (N.C.); konstantinos.spyrou1@gmail.com (K.S.); kovasil@auth.gr (K.C.V.); dmoschov@cc.uoi.gr (D.M.); aavger@uoi.gr (A.A.); chgioti@cc.uoi.gr (C.G.); mkarakas@uoi.gr (M.A.K.)

<sup>2</sup> Physics Department, University of Ioannina, 45110 Ioannina, Greece

\* Correspondence: bourlino@cc.uoi.gr (A.B.B.); dgourni@uoi.gr (D.G.); Tel.: +30-26510-07141 (D.G.)

Academic Editor: Giuseppe Cirillo

Received: 12 April 2020; Accepted: 6 May 2020; Published: 8 May 2020



**Abstract:** Recently we have highlighted the importance of hypergolic reactions in carbon materials synthesis. In an effort to expand this topic with additional new paradigms, herein we present novel preparations of carbon nanomaterials, such-like carbon nanosheets and fullerols (hydroxylated fullerenes), through spontaneous ignition of coffee-sodium peroxide ( $\text{Na}_2\text{O}_2$ ) and  $\text{C}_{60}$ - $\text{Na}_2\text{O}_2$  hypergolic mixtures, respectively. In these cases, coffee and fullerenes played the role of the combustible fuel, whereas sodium peroxide the role of the strong oxidizer (e.g., source of highly concentrated  $\text{H}_2\text{O}_2$ ). The involved reactions are both thermodynamically and kinetically favoured, thus allowing rapid product formation at ambient conditions. In addition, we provide tips on how to exploit the released energy of such highly exothermic reactions in the generation of useful work.

**Keywords:** hypergolic reactions; sodium peroxide; carbon nanosheets; fullerols; useful energy

## 1. Introduction

Carbon plays a central role in material science due to its variety of forms and enchanted properties [1]. Traditionally, carbon synthesis is an energy-consuming process that requires heating of an organic precursor in an oven at elevated temperature for certain periods of time. In this respect, the development of fast, spontaneous and energy-liberating (e.g., exothermic) preparative methods at ambient conditions would be of great value in carbon materials synthesis. Recently, we have introduced hypergolic reactions [2–4] as a useful tool in the rapid and spontaneous synthesis of a wide range of carbon nanomaterials at ambient conditions [5–7]. It is worth noting, the released energy from such highly exothermic reactions could be further exploited in the generation of useful work (chemical, mechanical, electrical, etc.). In one case, we have shown the formation of carbon nanosheets by the self-ignition of pyrophoric lithium dialkylamides salts in air, with the released energy being utilized for the generation of thermoelectric power [5]. In another case, the spontaneous ignition of an acetylene-chlorine mixture produced highly crystalline graphite at ambient conditions [6]. Lastly, hypergolic mixtures based on nitrile rubber or Girard's reagent T and fuming  $\text{HNO}_3$  as a strong oxidizer, led to the formation of carbon nanosheets or photoluminescent carbon dot respectively, with the released heat being utilized for the thermal transformation of a triazine precursor into graphitic carbon nitride or of coffee grains into a lightweight carbon absorbent [7].

In an effort to further build upon these results from our group, in the present work we provide additional new paradigms of hypergolic reactions in the service of carbon nanomaterials synthesis. Sodium peroxide  $\text{Na}_2\text{O}_2$  was used as a strong oxidizer [8], the latter being a source of highly

concentrated  $\text{H}_2\text{O}_2$  (a reactive oxygen species) upon contact with water. On the other hand, coffee [9,10] and fullerenes  $\text{C}_{60}$  acted as the carbon source in the corresponding hypergolic mixtures. As far as the carbon materials of interest is concerned here, these included carbon nanosheets [11] and fullerols (hydroxylated fullerenes) [12].

In a first paradigm, the ignition of instant coffee grains by  $\text{Na}_2\text{O}_2$  resulted in carbon nanosheets, the latter shown here to be an effective solar energy absorbent. Interestingly, the energy released from the reaction could be drain off to photovoltaics or to the preparation of important magnetic materials, such as magnetic iron oxides from the thermal decomposition of ferric acetate. In a second paradigm, simply crushing  $\text{C}_{60}$  in the presence of  $\text{Na}_2\text{O}_2$  caused ignition of the mixture with simultaneous formation of fullerols, a well-established fullerene derivative with interesting physico-chemical properties and numerous applications.

## 2. Results and Discussion

### 2.1. Carbon Nanosheets

The XRD pattern of the coffee-derived carbon nanosheets exhibited a very broad reflection centred at  $d_{002} = 3.9 \text{ \AA}$  (Figure 1, top), signalling the formation of amorphous carbon [13]. Likewise, Raman spectroscopy gave broad D ( $1355 \text{ cm}^{-1}$ ) and G ( $1590 \text{ cm}^{-1}$ ) bands with a relatively intensity ratio of  $I_D/I_G = 0.9$  (Figure 1, bottom), both being typical features of non-crystalline carbon [13]. On the other hand, the XPS spectrum of the nanosheets was identical to those reported in references 5 and 7 for oxidized carbon nanosheets. AFM study of the nanosheets showed the presence of large plates with thickness 1.5–2.5 nm (Figure 2, top). The morphology and size of the sheets were additionally confirmed by TEM microscopy (Figure 2, bottom).

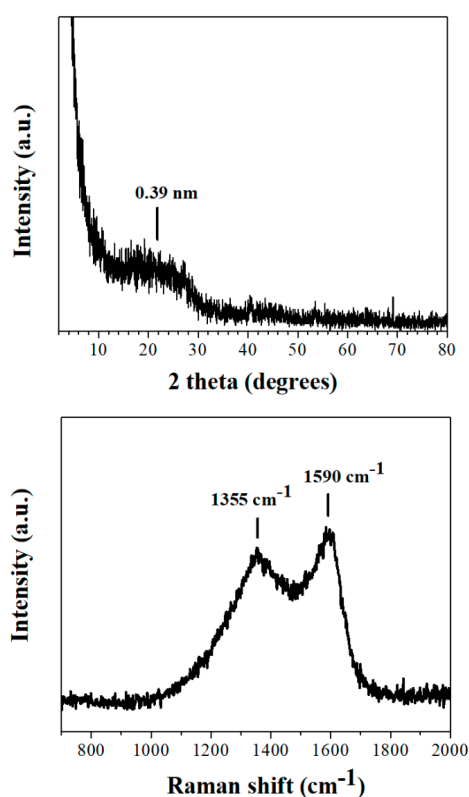


**Figure 1.** XRD pattern (top) and Raman spectrum (bottom) of the coffee-derived carbon nanosheets.

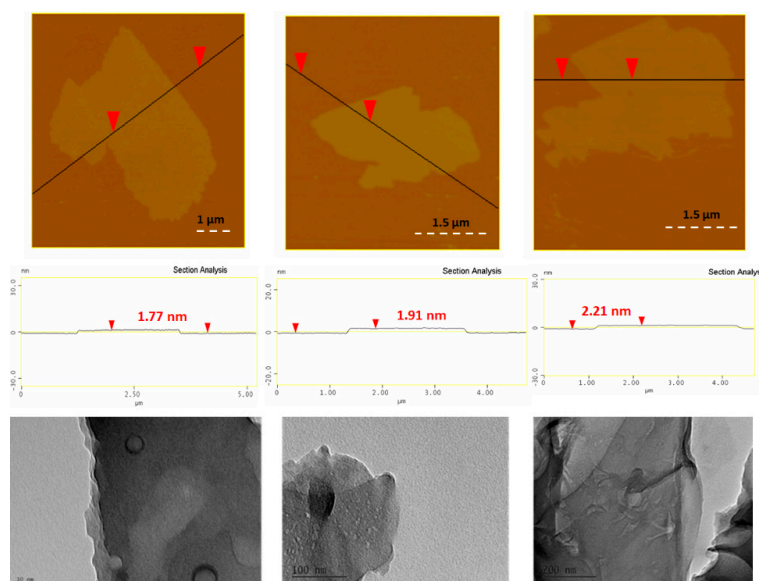


**Figure 2.** Top: AFM images of cross sectional analysis of selected carbon nanosheets. Bottom: representative TEM images of the sheets.

The  $N_2$  adsorption-desorption isotherms for the carbon nanosheets is shown in Figure 3. The sample exhibited isotherm of type I according to IUPAC classification, with a H4 type hysteresis loop which is characteristic of slit-shaped pores. The surface area of the sample and the total pore volume were calculated using BET equation ( $S_{BET}$ ) or alternatively, by the “t-plot” and Quenched Solid Density Functional Theory (QSDFT) methods. According to these methods the specific surface area was calculated to be  $130 \text{ m}^2/\text{g}$  ( $S_{BET}$ ),  $164 \text{ m}^2/\text{g}$  ( $S_t$ , t-plot) and  $179 \text{ m}^2/\text{g}$  (QSDFT) respectively, whereas the total pore volume found to be  $0.06 \text{ cm}^3/\text{g}$  (cumulative at  $P/P_0 = 0.97$ ),  $0.06 \text{ cm}^3/\text{g}$  (t-plot) and  $0.085 \text{ cm}^3/\text{g}$  (QSDFT). From the pore size distribution PSD (inset) according to the QSDFT model (Figure S1), carbon nanosheets seemed to exhibit micropores with two average sizes 1.2 nm and 1.7 nm and mesoporous 3.7 nm. However, the volume analysis from “t-plot” (Figure S2) showed only the presence of micropores in agreement with classification type of adsorption isotherm. It is obvious that the observed step down in the desorption branch between relative pressures 0.4 to 0.6 (Figure 3), is responsible for the observed mesoporous peak in the calculated PSD. That peak is probably an artefact, caused by the spontaneous evaporation of metastable pore liquid (i.e., cavitation). Besides, H3 or H4 hysteresis is often attributed to the occurrence of pore blocking and percolation phenomena and it is not only associated with the pore condensation [14]. From a practical point of view, the surface area of the nanosheets in combination with the oxygen functionalities present on their surface could make the material useful in adsorption processes (e.g., removal of heavy metals or dyes from water).

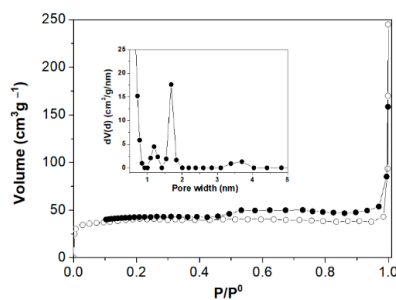


**Figure 3.**  $N_2$  adsorption-desorption isotherms of carbon nanosheets. Inset: Quenched Solid Density Functional Theory (QSDFT) pore size distribution.

The black solid could be used as a pigment in water glass paints for solar energy harvesting. Water glass refers to an aqueous solution of the inorganic polymer sodium silicate (40%, Aldrich) that can wrap and electrostatically stabilize any dispersed solid. To this aim, carbon nanosheets were simply mechanically mixed with water glass to create the paint. The paint was then spread over a piece of paper with a brush and left to dry at room temperature (see the corresponding black square drawing in Figure 4, top). A similar drawing using an analogous CuO paint was also sketched in a separate piece of paper (Figure 4, top); cupric oxide is a reference black pigment that is often used in solar water heaters [15]. Following, both coatings were illuminated under an infrared lamp at the same distance and for the same time (20 s) prior to scanning with a thermal camera. As it can be seen from the thermal camera images in Figure 4, bottom, carbon nanosheets and cupric oxide developed comparable temperatures (100–120 °C) under identical conditions. Hence, thanks to their flat surface and blackness, the coffee-derived carbon nanosheets could be promising solar energy absorbents [16]. It should be noted that although the CuO film seems homogeneously darker, the nanosheets yield higher temperature rise in places that appear even darker due to a higher mass of deposited material. Thus, the temperature distribution as presented is valid.

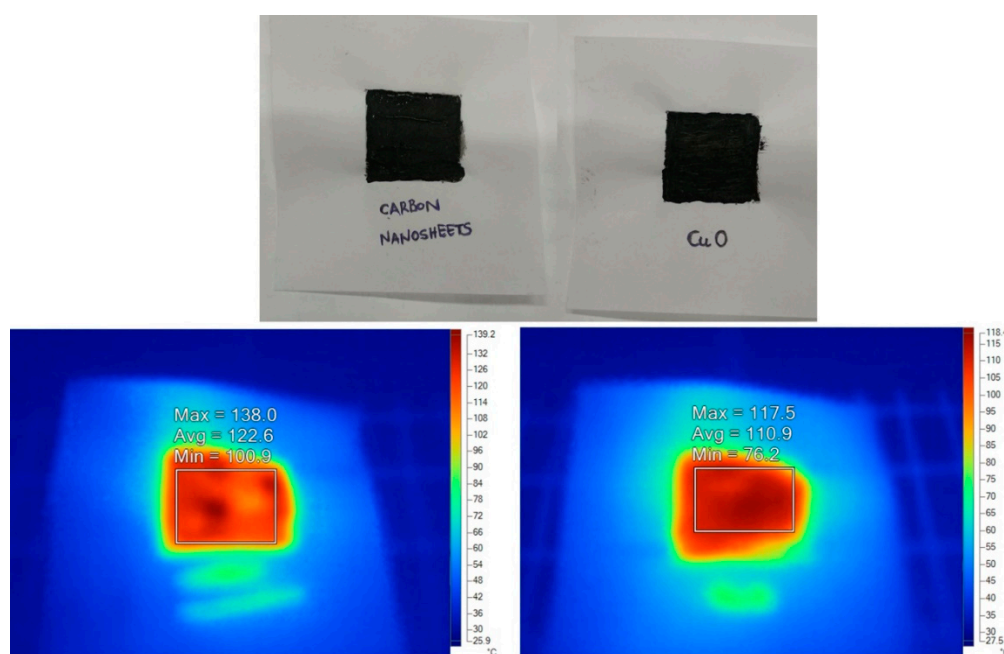


**Figure 4.** Top: dry carbon nanosheet and CuO paints on paper sheet (black squares). Bottom: the corresponding thermal camera images after 20 s illumination with infrared lamp (left: carbon nanosheets; right: CuO). Both samples developed comparable temperature after illumination under identical conditions, thus demonstrating that the coffee-derived carbon nanosheets are effective solar energy absorbents.

The heat and light produced from the reaction of the coffee grains with  $\text{Na}_2\text{O}_2$  was utilized in the generation of useful work. In one example, a miniature silicon photovoltaic panel connected with a green LED light was placed above the ignition mixture with the front side facing down the mixture at certain distance (Figure 5, top). The band-gap energy of silicon is 1.1 eV, the latter corresponding to the infrared part of the electromagnetic radiation. Upon ignition, the thermal radiation and light produced from the flame turned on the LED light (Figure 5, top), thus acting as a sort of thermophotovoltaic [17]. In another example, the heat produced from the hypergolic mixture was exploited in the thermal decomposition of ferric acetate into magnetic iron oxide [18,19]. For this purpose, a quartz tube charged with ferric acetate was dipped into an alumina crucible containing the hypergolic mixture (Figure 5,

bottom). Ignition of the mixture provided the necessary heat for the thermal decomposition of the precursor inside the tube into magnetic iron oxide (Figure 5, bottom).



**Figure 5.** Top: ignition of the coffee- $\text{Na}_2\text{O}_2$  mixture generates enough thermal radiation and light to turn on a miniature silicon photovoltaic device. Bottom: the ignitable mixture served as a heat source for the in-situ thermal transformation of ferric acetate (orange powder at far-left) into magnetic iron oxide (black solid at far-right). For this purpose, a small quartz tube was charged with the precursor and then merely dipped into the ignition mixture. Notice the release of smoke from the top rim of the tube due to thermal decomposition of ferric acetate.

## 2.2. Fullerenols

The ignition of coffee by sodium peroxide presented above is considered a classic demonstration experiment in the area of hypergolic reactions that, as shown here, results in carbon nanosheets. Another interesting hypergolic mixture reported for first time is the  $\text{C}_{60}$ - $\text{Na}_2\text{O}_2$  system (Figure 10). Although several carbon allotropes and their derivatives have been used as booster additives in hypergolic fuels [20], however, it is very seldom to observe spontaneous ignition between elemental carbon and a strong oxidizer upon direct contact. Perhaps a sole example in the literature refers to the activated charcoal- $\text{Na}_2\text{O}_2$  pair [8] (see also *Bretherick's Handbook of Reactive Chemical Hazards*). Hence, the  $\text{C}_{60}$ - $\text{Na}_2\text{O}_2$  system adds another example in the list, thus paving the way for the advancement of novel hypergolics strictly based on carbon. It should be mentioned that similar treatment of other carbon allotropes (e.g., nanodiamonds, carbon nanotubes) with  $\text{Na}_2\text{O}_2$  gave no ignition. Apparently, the small size and strain of fullerenes make them prone to ignition.

The  $\text{C}_{60}$ - $\text{Na}_2\text{O}_2$  system is of synthetic value as well, since it can afford fullerols, an important hydroxylated fullerene derivative. In general, the formation of fullerols from  $\text{C}_{60}$  requires the simultaneous presence of  $\text{H}_2\text{O}_2$  and  $\text{NaOH}$  [21]. In our case, both chemicals were released in-situ by the peroxide hydrolysis in humid air (e.g.,  $\text{Na}_2\text{O}_2 + 2 \text{H}_2\text{O} \rightarrow \text{H}_2\text{O}_2 + 2 \text{NaOH}$ ). The ATR-IR spectrum of the dark brown solid derived from the reaction displayed several broad bands of moderate intensity at  $3450 \text{ cm}^{-1}$  (O-H),  $<3000 \text{ cm}^{-1}$  (aliphatic C-H),  $1717 \text{ cm}^{-1}$  (C=O),  $1618 \text{ cm}^{-1}$  (enol C=C) and  $1045 \text{ cm}^{-1}$  (C-O) (Figure 6, top). The sharp peaks at  $1183 \text{ cm}^{-1}$  and  $1427 \text{ cm}^{-1}$  are ascribed to unreacted  $\text{C}_{60}$ , which cannot be completely removed by further washing (e.g., with toluene). This issue should be cautiously taken into consideration upon scaling-up synthesis. These observations are similar to

those reported by Afreen et al. elsewhere for fullerol formation from  $C_{60}$  [22]. Especially the O-H, enol C=C and C-O stretchings at  $3450\text{ cm}^{-1}$ ,  $1618\text{ cm}^{-1}$  and  $1045\text{ cm}^{-1}$  respectively, are indicative of the attachment of -OH groups onto the  $C_{60}$  cage. Of particular interest is the appearance of aliphatic C-H and carbonyl C=O bands in the spectrum. The carbonyl group is often ascribed in the literature to the pinacol-pinacolone rearrangement in fullerene 1,2-diols [23]. However, such rearrangement seems rather unlikely for fullerenes since it would require the movement of a fixed skeletal carbon within the cage. In addition, it cannot explain the appearance of C-H aliphatics in the spectrum. Hence, these bands should be better ascribed to the keto-enol tautomerism, which simpler involves the movement of a hydrogen atom from the hydroxyl group of C=C-OH (enol form) to an alpha carbon (e.g., H-C-C=O, keto form). In this way, both C-H and C=O bands can be rationalized in the spectrum. According to TGA under  $N_2$  (Figure 6, bottom), fullerol exhibited a first weight loss below  $150\text{ }^\circ\text{C}$  due to the release of hydration water (ca. 8%  $w/w$ ) and another one between 150 and  $600\text{ }^\circ\text{C}$  due to dehydroxylation of the cluster (ca. 13%  $w/w$ ) [24]. These weight losses agree with the formula  $C_{60}(\text{OH})_{7.4}\text{H}_2\text{O}$ , i.e., low-hydroxylated fullerol [25]. It is worth noting, the latter formula is close to that of  $C_{60}(\text{OH})_8 \cdot 2\text{H}_2\text{O}$  previously reported by Afreen et al. [22].

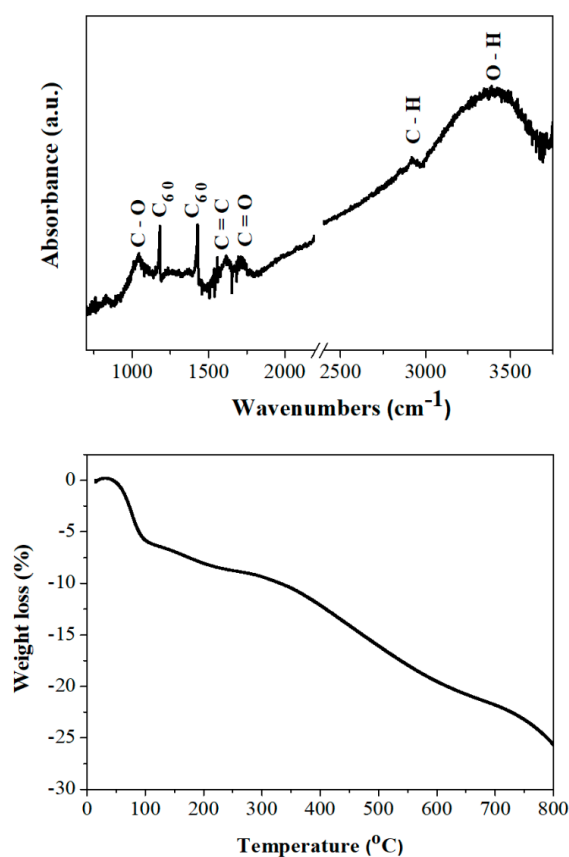


**Figure 6.** Top: ATR-IR spectrum of the fullerols. Bottom: the corresponding thermogravimetric analysis (TGA) trace under  $N_2$ .

AFM study of the aqueous-dispersed solid revealed the presence of large globular nanoparticles with size in the range of 15–25 nm (Figure 7). Fullerol typically has a size of 1.5 nm; however, it is well-known to form larger aggregates and eventually fullerol nanoparticles (10–60 nm) as a result of strong hydrogen bonding and  $\pi$ - $\pi$  interactions between adjacent clusters [26].

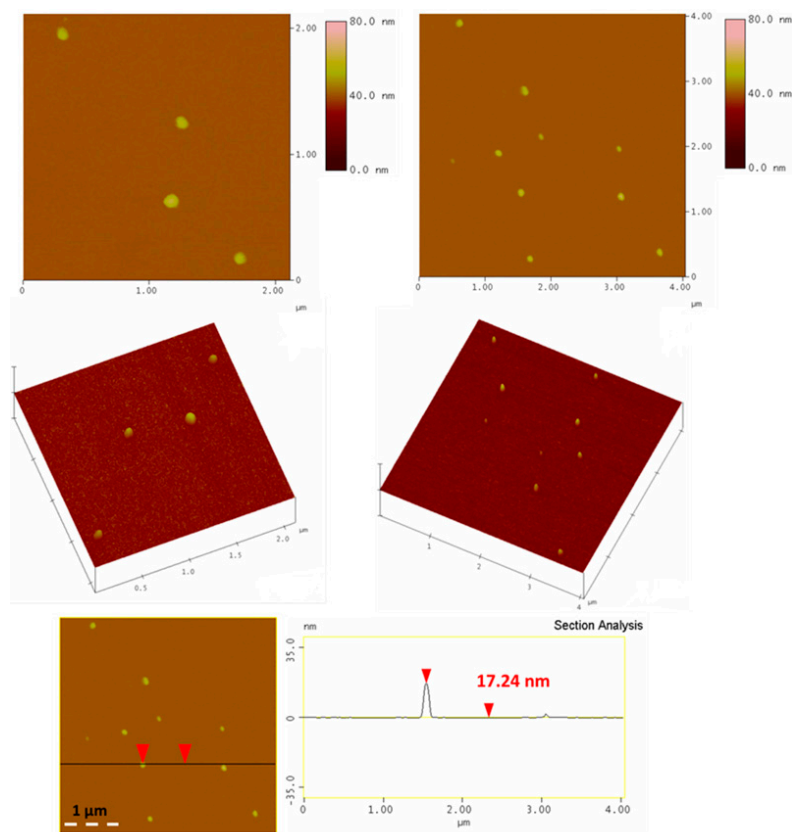


**Figure 7.** Representative AFM height images (top), 3D morphology (middle) and cross section analysis profile (bottom) of the globular fullerol nanoparticles.

High resolution C1s XPS gave useful information about the structure of the synthesized fullerols (Figure 8). The dominant peak at 285.2 eV is due to the carbon cage of the fullerols [27]. Additionally, the shake-up features associated with the C<sub>60</sub>-cage atoms were identified at 288.5 eV and 291.2 eV [28,29]. On the other hand, the small fraction of sp<sup>3</sup> carbons observed at 284.2 eV is consistent with a low degree of functionalization (e.g., low-hydroxylated fullerols). The peak at 286.0 eV is typical of hydroxyl C-OH groups, whereas those at 287.2 and 289.9 eV of C=O/C-O-C/C(O)O species [30]. Lastly, the feature at 283.0 eV is ascribed to iron carbides, the latter resulting from iron contamination of the sample by the metallic container used for reaction.

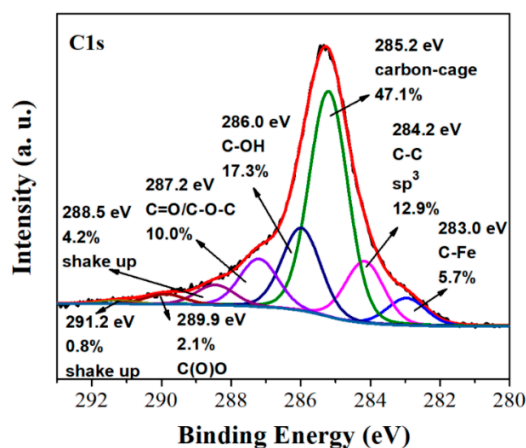


**Figure 8.** C1s photoelectron spectrum of fullerols.

To sum-up, the ATR-IR, TGA, AFM and XPS data are well-consistent with the formation of low-hydroxylated fullerol, a useful precursor to higher fullerols.

### 3. Materials and Methods

For safety reasons all experiments were conducted in a fume hood with ceramic tiles bench.

#### 3.1. Carbon Nanosheets

2 g of instant coffee grains (Nescafe®) were mixed with 2 g  $\text{Na}_2\text{O}_2$  beads (93%, Sigma-Aldrich, St. Louis, MO, USA) in a porcelain dish followed by the quick addition of 1 mL water. Ignition started with a short delay (30–45 s after water addition) giving off an intense yellow flame due to the sodium ions present. The reaction led to a crude carbon residue after cooling of the product. Thorough washings with water, dimethylformamide (DMF) and acetone afforded a fine black powder containing carbon nanosheets (yield: 2%). The whole process is visualized in Figure 9. Any minor inorganic contaminants due to the porcelain dish were removed by treating the sample with 48% HF aqueous solution.



**Figure 9.** Left-to-right: instant coffee grains were mixed with  $\text{Na}_2\text{O}_2$  beads in a porcelain dish. Subsequent addition of water caused ignition of the mixture towards the formation of a crude carbon residue. After thorough washings, a fine black powder was obtained containing carbon nanosheets.

#### 3.2. Fullerenols

150 mg of  $\text{C}_{60}$  powder (98%, Sigma-Aldrich, St. Louis, MO, USA) were crushed in the presence of 1.7 g  $\text{Na}_2\text{O}_2$  beads (93%, Sigma-Aldrich, St. Louis, MO, USA) using a stainless steel mortar and pestle. Due to rapid oxidation of the carbon clusters by the peroxide, the mixture ignited spontaneously within few seconds. The product washed successively with concentrated HCl aqueous solution (37%) in order to remove excess of  $\text{Na}_2\text{O}_2$  (slow addition), water, and finally acetone. A fine dark brown powder was obtained made up of fullerol clusters (yield: 10%). The clusters were soluble in water by alkaline treatment with NaOH and sonication, due to neutralization of the acidic phenolic protons into phenolate ionic groups [12]. The whole process is visualized in Figure 10. It should be mentioned that the stainless steel mortar and pestle was used in order to crush the very hard  $\text{Na}_2\text{O}_2$  beads. Also, no ignition was observed upon crushing the  $\text{Na}_2\text{O}_2$  beads inside the metallic container in the absence of fullerenes, suggesting that no reaction is taking place between the peroxide and the walls of the metallic container.



**Figure 10.** Crushing fullerenes in the presence of  $\text{Na}_2\text{O}_2$  in a stainless steel mortar and pestle caused ignition of the mixture as evidenced by the generation of bright flash. Washing of the product led to a dark brown powder, namely fullerols. Fullerols were soluble in water by mild alkaline treatment and sonication.

At this point we would like to first emphasize that the yields of the above reactions, although low at first glance, are generally considered fair enough in materials science. Second, the selection of a combustible material is rather a trial and error effort at this stage. Several other organic compounds were tested in our lab but failed ignition with sodium peroxide. In many cases though, the reagents reacted exothermically without giving off flame. We speculate that the quantity of mixed reactants play a key role for ignition. Third, the reported hypergolic pairs are unique in terms of matching. For instance, the reaction of coffee grains or C<sub>60</sub> with fuming HNO<sub>3</sub> (100%), though exothermic, gave no ignition.

Powder X-ray diffraction (XRD) was performed using background-free Si wafers and Cu K $\alpha$  radiation from a Bruker Advance D8 diffractometer (Bruker, Billerica, MA, USA). Raman spectra were recorded with a RM 1000 Renishaw micro-Raman system using a laser excitation line at 532 nm (Renishaw, Wotton-under-Edge, England). Attenuated total reflection infrared spectroscopy (ATR-IR) measurements were performed using a Jasco IRT-5000 microscope coupled with a FT/IR-4100 spectrometer (Jasco, Easton, MD, USA). The ZnSe prism of the ATR objective had a 250  $\mu$ m area in contact with the sample. Background was subtracted and the baseline was corrected for all spectra. Thermogravimetric analysis (TGA) was performed using a Perkin Elmer Pyris Diamond TG/DTA (PerkinElmer, Inc., Waltham, MA, USA). The fullerol sample was heated under N<sub>2</sub> flow at a rate of 5 °C min<sup>-1</sup>. X-ray photoelectron spectroscopy (XPS) measurements were performed in an ultra-high vacuum at a base pressure of 4  $\times$  10<sup>-10</sup> mbar with a SPECS GmbH spectrometer equipped with a monochromatic Mg K $\alpha$  source (h $\nu$  = 1253.6 eV) and a Phoibos-100 hemispherical analyser (Berlin, Germany). Spectral analysis included a Shirley background subtraction and peak separation using Gaussian-Lorentzian functions in a least square fitting program (Winspec) developed at the LISE laboratory, University of Namur, Belgium. The N<sub>2</sub> adsorption-desorption isotherms were measured at 77 K on a Sorptomatic 1990, ThermoFinnigan porosimeter (Thermo Finnigan LLC, San Jose, CA, USA). Carbon nanosheets were outgassed at 150 °C for 20 h under vacuum before measurements. Specific surface areas were determined with the Brunauer–Emmett–Teller (BET) method. Atomic force microscopy (AFM) images were collected in tapping mode with a Bruker Multimode 3D Nanoscope (Ted Pella Inc., Redding, CA, USA) using a microfabricated silicon cantilever type TAP-300G, with a tip radius of <10 nm and a force constant of approximately 20–75 N m<sup>-1</sup>. The transmission electron microscopy (TEM) study of carbon nanosheets deposited on carbon coated copper grids (CF300-CU-UL, carbon square mesh, CU, 300 mesh from Electron Microscopy Science) was performed using the instrument JEM HR-2100, JEOL Ltd., Tokyo, Japan operated at 200 kV in bright-field mode.

#### 4. Conclusions

We have presented new hypergolic reactions towards the synthesis of functional carbon nanomaterials, such-like carbon nanosheets and fullerols. The new systems composed of coffee or fullerene as the combustible fuel and sodium peroxide as the strong oxidizer. In all instances, synthesis was fast, spontaneous and exothermic at ambient conditions, thus enabling not only facile carbon formation but also the generation of useful work (herein photovoltaic or chemical). The coffee-derived carbon nanosheets, due to their flat surface and blackness, seemed to serve as an effective solar energy absorbent, whereas fullerols itself is a well-known fullerene derivative with important properties and uses. Overall, the present work builds upon previous results from our group, showing altogether the wider applicability and generic character of hypergolic reactions in carbon materials synthesis.

**Supplementary Materials:** The following are available online at <http://www.mdpi.com/1420-3049/25/9/2207/s1>, Figure S1: Fitting comparison between experimental data of carbon nanosheets and QSDFT model (N<sub>2</sub>, carbon equilibrium transition kernel at 77 K based on a slit pore model), Figure S2: t-plot for nitrogen adsorbed at 77 K in carbon nanosheets.

**Author Contributions:** Conceptualization, experiments and writing A.B.B. and D.G.; characterization, formal analysis, and writing N.C., K.S., K.C.V., D.M., A.A., C.G. and M.A.K. All authors have read and agreed to the published version of the manuscript.

**Funding:** We acknowledge support of this work by the project “National Infrastructure in Nanotechnology, Advanced Materials and Micro-/Nanoelectronics” (MIS 5002772) which is implemented under the Action “Reinforcement of the Research and Innovation Infrastructure”, funded by the Operational Programme “Competitiveness, Entrepreneurship and Innovation” (NSRF 2014-2020) and co-financed by Greece and the European Union (European Regional Development Fund). This research is also co-financed by Greece and the European Union (European Social Fund- ESF) through the Operational Programme “Human Resources Development, Education and Lifelong Learning” in the context of the project “Strengthening Human Resources Research Potential via Doctorate Research” (MIS-5000432), implemented by the State Scholarships Foundation (IKY).

**Acknowledgments:** The authors greatly acknowledge Ch. Papachristodoulou for the XRD measurements and lab technician P. Triantafyllou for the construction of the silicon photovoltaic.

**Conflicts of Interest:** The authors declare no conflict of interest.

## References

1. Georgakilas, V.; Perman, J.A.; Tucek, J.; Zboril, R. Broad Family of Carbon Nanoallotropes: Classification, Chemistry, and Applications of Fullerenes, Carbon Dots, Nanotubes, Graphene, Nanodiamonds, and Combined Superstructures. *Chem. Rev.* **2015**, *115*, 4744–4822. [CrossRef] [PubMed]
2. Hypergolic Propellant. Available online: [https://en.wikipedia.org/wiki/Hypergolic\\_propellant](https://en.wikipedia.org/wiki/Hypergolic_propellant) (accessed on 28 December 2019).
3. Silva, G.D.; Iha, K. Hypergolic Systems: A Review in Patents. *J. Aerosp. Technol. Manag.* **2012**, *4*, 407–412. [CrossRef]
4. Schneider, S.; Hawkins, T.; Rosander, M.; Vaghjani, G.; Chambreau, S.; Drake, G. Ionic Liquids as Hypergolic Fuels. *Energy Fuels* **2008**, *22*, 2871–2872. [CrossRef]
5. Baikousi, M.; Chalmpes, N.; Spyrou, K.; Bourlinos, A.B.; Avgeropoulos, A.; Gournis, D.; Karakassides, M.A. Direct production of carbon nanosheets by self-ignition of pyrophoric lithium dialkylamides in air. *Mater. Lett.* **2019**, *254*, 58–61. [CrossRef]
6. Chalmpes, N.; Spyrou, K.; Bourlinos, A.B.; Moschovas, D.; Avgeropoulos, A.; Karakassides, M.A.; Gournis, D. Synthesis of Highly Crystalline Graphite from Spontaneous Ignition of In Situ Derived Acetylene and Chlorine at Ambient Conditions. *Molecules* **2020**, *25*, 297. [CrossRef] [PubMed]
7. Chalmpes, N.; Asimakopoulos, G.; Spyrou, K.; Vasilopoulos, K.C.; Bourlinos, A.B.; Moschovas, D.; Avgeropoulos, A.; Karakassides, M.A.; Gournis, D. Functional Carbon Materials Derived through Hypergolic Reactions at Ambient Conditions. *Nanomaterials* **2020**, *10*, 566. [CrossRef]
8. Sodium Peroxide + Cornflakes + Milk = Explosion! Available online: <https://www.youtube.com/watch?v=M57TOMvsNsI> (accessed on 1 February 2018).
9. Wen, X.; Liu, H.; Zhang, L.; Zhang, J.; Fu, C.; Shi, X.; Chen, X.; Mijowska, E.; Chen, M.-J.; Wang, D.-Y. Large-scale converting waste coffee grounds into functional carbon materials as high-efficient adsorbent for organic dyes. *Bioresour. Technol.* **2019**, *272*, 92–98. [CrossRef]
10. Gao, G.; Cheong, L.-Z.; Wang, D.; Shen, C. Pyrolytic carbon derived from spent coffee grounds as anode for sodium-ion batteries. *Carbon Resour. Convers.* **2018**, *1*, 104–108. [CrossRef]
11. Fan, H.; Shen, W. Carbon Nanosheets: Synthesis and Application. *ChemSusChem* **2015**, *8*, 2004–2027. [CrossRef]
12. Vileno, B.; Marcoux, P.R.; Lekka, M.; Sienkiewicz, A.; Fehér, T.; Forró, L. Spectroscopic and Photophysical Properties of a Highly Derivatized C60 Fullerol. *Adv. Funct. Mater.* **2006**, *16*, 120–128. [CrossRef]
13. Roh, J.-S. Structural Study of the Activated Carbon Fiber Using Laser Raman Spectroscopy. *Carbon Lett.* **2008**, *9*, 127–130. [CrossRef]
14. Thommes, M. Physical Adsorption Characterization of Nanoporous Materials. *Chem. Ing. Tech.* **2010**, *82*, 1059–1073. [CrossRef]
15. Karthick Kumar, S.; Suresh, S.; Murugesan, S.; Raj, S.P. CuO thin films made of nanofibers for solar selective absorber applications. *Sol. Energy* **2013**, *94*, 299–304. [CrossRef]
16. Jönsson, G.; Fredriksson, H.; Sellappan, R.; Chakarov, D. Nanostructures for Enhanced Light Absorption in Solar Energy Devices. *Int. J. Photoenergy* **2011**, *2011*, 939807.

17. Coutts, T.J. A review of progress in thermophotovoltaic generation of electricity. *Renew. Sustain. Energy Rev.* **1999**, *3*, 77–184. [[CrossRef](#)]
18. Jewur, S.S.; Kuriacose, J.C. Studies on the thermal decomposition of ferric acetate. *Thermochim. Acta* **1977**, *19*, 195–200. [[CrossRef](#)]
19. Pinheiro, E.A.; Pereira de Abreu Filho, P.; Galembeck, F.; Correa da Silva, E.; Vargas, H. Magnetite crystal formation from iron(III) hydride acetate. An ESR study. *Langmuir* **1987**, *3*, 445–448. [[CrossRef](#)]
20. Yan, Q.-L.; Gozin, M.; Zhao, F.-Q.; Cohen, A.; Pang, S.-P. Highly energetic compositions based on functionalized carbon nanomaterials. *Nanoscale* **2016**, *8*, 4799–4851. [[CrossRef](#)]
21. Wang, S.; He, P.; Zhang, J.M.; Jiang, H.; Zhu, S.Z. Novel and Efficient Synthesis of Water-Soluble [60]Fullerenol by Solvent-Free Reaction. *Synth. Commun.* **2005**, *35*, 1803–1808. [[CrossRef](#)]
22. Afreen, S.; Kokubo, K.; Muthoosamy, K.; Manickam, S. Hydration or hydroxylation: Direct synthesis of fullerenol from pristine fullerene [C60] via acoustic cavitation in the presence of hydrogen peroxide. *RSC Adv.* **2017**, *7*, 31930–31939. [[CrossRef](#)]
23. Meier, M.S.; Kiegiel, J. Preparation and Characterization of the Fullerene Diols 1,2-C60(OH)2, 1,2-C70(OH)2, and 5,6-C70(OH)2. *Org. Lett.* **2001**, *3*, 1717–1719. [[CrossRef](#)] [[PubMed](#)]
24. Goswami, T.H.; Singh, R.; Alam, S.; Mathur, G.N. One-Pot Synthesis of a Novel Water-Soluble Fullerene-Core Starlike Macromolecule via Successive Michael and Nucleophilic Addition Reaction. *Chem. Mater.* **2004**, *16*, 2442–2448. [[CrossRef](#)]
25. Kokubo, K. Water-Soluble Single-Nano Carbon Particles: Fullerenol and Its Derivatives. In *The Delivery of Nanoparticles*; InTech: London, UK, 2012.
26. Djordjevic, A.; Srdjenovic, B.; Seke, M.; Petrovic, D.; Injac, R.; Mrđanović, J. Review of Synthesis and Antioxidant Potential of Fullerenol Nanoparticles. *J. Nanomater.* **2015**, *2015*, 567073. [[CrossRef](#)]
27. Maxwell, A.J.; Brühwiler, P.A.; Nilsson, A.; Mårtensson, N.; Rudolf, P. Photoemission, autoionization, and x-ray-absorption spectroscopy of ultrathin-film C60 on Au(110). *Phys. Rev. B* **1994**, *49*, 10717–10725. [[CrossRef](#)]
28. Enkvist, C.; Lunell, S.; Sjögren, B.; Brühwiler, P.A.; Svensson, S. The C1s shakeup spectra of Buckminsterfullerene, acenaphthylene, and naphthalene, studied by high resolution x-ray photoelectron spectroscopy and quantum mechanical calculations. *J. Chem. Phys.* **1995**, *103*, 6333–6342. [[CrossRef](#)]
29. Leiro, J.A.; Heinonen, M.H.; Laiho, T.; Batirev, I.G. Core-level XPS spectra of fullerene, highly oriented pyrolytic graphite, and glassy carbon. *J. Electron Spectrosc. Relat. Phenom.* **2003**, *128*, 205–213. [[CrossRef](#)]
30. Felicissimo, M.; Jarzab, D.; Gorgoi, M.; Forster, M.; Scherf, U.; Scharber, M.; Svensson, S.; Rudolf, P.; Loi, M. Determination of vertical phase separation in a polyfluorene copolymer: Fullerene derivative solar cell blend by X-ray photoelectron spectroscopy. *J. Mater. Chem.* **2009**, *19*, 4899–4901. [[CrossRef](#)]

**Sample Availability:** Samples of the compounds are not available from the authors.



© 2020 by the authors. Licensee MDPI, Basel, Switzerland. This article is an open access article distributed under the terms and conditions of the Creative Commons Attribution (CC BY) license (<http://creativecommons.org/licenses/by/4.0/>).